RSC Advances

PAPER

View Article Online
View Journal | View Issue

Cite this: *RSC Adv.*, 2017, **7**, 6957

One-step solvothermal synthesis of interlaced nanoflake-assembled flower-like hierarchical Ag/Cu_2O composite microspheres with enhanced visible light photocatalytic properties†

Yongxing Zhang,‡[a] Xiangbo Zhou,‡[a] Yuanyuan Zhao,[a] Zhongliang Liu,[a] Dong Ma,[a] San Chen,[a] Guangping Zhu[a] and Xuanhua Li*[bc]

Three-dimensional (3D) micro/nano hierarchical structure semiconductor catalysts not only inherit the excellent properties of single nanometer-size building blocks resulting from their high specific surface area and high activity but also provide the merits of high dispersion and easy recovery of microstructures. Herein, the interlaced nanoflake-assembled flower-like hierarchical Ag/Cu_2O composite microspheres have been prepared *via* a one-step, environmentally friendly solvothermal method. Such interlaced nanoflake-assembled flower-like hierarchical Ag/Cu_2O composite microspheres show an excellent photocatalytic activity, which is 121 times faster than that of the commercial Cu_2O powders, and is one of the highest reported to date in the Ag/Cu_2O composite materials for the degradation of Methyl Orange (MO) under visible light illumination. Our experimental results for photodegradation of MO also indicate that the existence of Cu in the products does not favor high photocatalytic activity for Ag/Cu_2O composites, which may be due to the existence of excess metal in the products which provides the recombination centers for electron–hole pairs. After five consecutive cycles, the photocatalytic activity of the interlaced nanoflake-assembled flower-like hierarchical Ag/Cu_2O composite microspheres almost remains unchanged, indicating that they are photostable during the photodegradation of MO. Most importantly, such micrometer-sized overall structures of the interlaced nanoflake-assembled flower-like hierarchical Ag/Cu_2O composite microspheres enable them to be recycled and reused easily from solution by natural settlement in a short time. These results suggest that the interlaced nanoflake-assembled flower-like hierarchical Ag/Cu_2O composite microspheres had potential applications in visible light photocatalysis for environmental remediation.

Received 16th November 2016
Accepted 12th January 2017

DOI: 10.1039/c6ra26870f

www.rsc.org/advances

1 Introduction

It is well known that semiconductor photocatalysts with nanometer size display excellent catalytic activity resulting from their high specific surface area and high activity.[1–5] However, easy agglomeration is one of the biggest drawbacks of these materials, which causes a sharp decline in the photocatalytic activity.[6] In addition, finely nanometer-sized catalysts are very difficult to recycle from the liquid system, resulting in low utilization and recontamination. Considering these shortcomings of nanometer-size catalysts, more attention has been paid to assemble low-dimensional nanometer-size building blocks (such as nanoparticles, nanowires, nanotubes, and nanoflakes) into three-dimensional (3D) micro/nano hierarchical structure semiconductor catalysts.[7–9] Such 3D micro/nano hierarchical structure semiconductor catalysts not only inherit the excellent properties of the single nanometer-size building blocks resulting from their high specific surface area and high activity but also provide the merits of high dispersion and easy recovery of microstructures.[10–13]

Cuprous oxide (Cu_2O) is a p-type metal oxide semiconductor with a direct band gap of 2.0–2.2 eV, which makes it a potentially promising photocatalyst for the photochemical decomposition of water into O_2 and H_2 and photocatalytic degradation of organic pollutants under visible light illumination.[14–17] However, pure Cu_2O exhibits very poor quantum efficiency because of the easy recombination between electron and hole.[18] To overcome this limitation, modification of Cu_2O

[a]*Collaborative Innovation Center of Advanced Functional Composites, Huaibei Normal University, Huaibei 235000, P. R. China*

[b]*State Key Laboratory of Solidification Processing Center of Nano Energy Materials, School of Materials Science and Engineering, Northwestern Polytechnical University, Xi'an 710072, P. R. China. E-mail: lixh32@nwpu.edu.cn*

[c]*Key Laboratory of Materials Physics, Institute of Solid State Physics, Chinese Academy of Sciences, Hefei 230031, P. R. China*

† Electronic supplementary information (ESI) available. See DOI: 10.1039/c6ra26870f

‡ These authors contributed equally to this work.

with noble metals (Ag, Au, Pt or Pd) is one of the most efficient ways.[19–22] This is mainly due to the fact that the noble metals can act as electron sinks due to the schottky barrier at the metal–semiconductor interface, while the photo induced holes can remain on the semiconductor surface.[23,24] Therefore, the recombination of the electrons and holes can be prevented, and the photocatalytic efficiency of semiconductor is improved. In addition, compared with other noble metals (Au, Pt and Pd), Ag is more attractive because of its high electrical, low cost, and nontoxicity.[25–29] It is widely accepted that Ag nanostructures exhibit a wealth of optical and photoelectrochemical properties directly related to their geometry dependent surface plasmon resonances, which make them great potential candidates in the field of photocatalysis.[30] So, there have been many outstanding studies on the preparation of Ag/Cu_2O composites for photocatalytic degradation of organic pollutants in wastewater. Li *et al.* reported the synthesis of Ag nanodisk–Cu_2O hybrid nanoconcaves through site-selective growth of noble metals on Cu_2O seeds for an effective synergistic catalyst.[30] Xiong *et al.* presented a method for rapid fabricating 1D Ag@Cu_2O core–shell heteronanowires for photodegradation of organic dyes.[31] Wu *et al.* successfully prepared the Ag core@Cu_2O shell architecture exhibiting the plasmonic enhancement of visible-light photocatalytic activity.[32] Wang *et al.* presented the M/Cu_2O (M = Ag, Au) octahedral nanocrystals with enhanced photocatalytic efficiency.[33] However, most of these methods suffer from the limitations of requiring longer reaction times, two reaction steps, presence of toxic reducing agents—$N_2H_4 \cdot 3H_2O$, for example. Thus, it still remains a challenge to develop a one-step, environmentally friendly solvothermal method for obtaining interlaced nanoflake-assembled flower-like hierarchical Ag/Cu_2O composite microspheres with enhanced visible light photocatalytic properties.

In this work, we designed a one-step, environmentally friendly solvothermal method to synthesize a interlaced nanoflake-assembled flower-like hierarchical Ag/Cu_2O composite microspheres at 180 °C for 1 h, employing ethylene glycol (EG) as a solvent, $Cu(NO_3)_2 \cdot 3H_2O$ and $AgNO_3$ as reagents in the presence of polyvinylpyrrolidone (PVP) as surfactant. To the best of our knowledge, this is the first report on the fabrication and photocatalytic capacity of interlaced nanoflake-assembled flower-like hierarchical Ag/Cu_2O composite microspheres *via* a one-step, environmentally friendly solvothermal method. Most importantly, the preparation of the interlaced nanoflake-assembled flower-like hierarchical Ag/Cu_2O composite microspheres in the efficient photocatalytic degradation of organic pollutants from water has the following features: (1) both Ag^+ and Cu^{2+} are reduced simultaneously by EG in our reaction system to form Ag/Cu_2O composites; (2) the existence of Cu in the products does not favor high photocatalytic activity for Ag/Cu_2O composites under visible light illumination. And the photocatalytic activity gradually decreases with increasing Cu content; (3) such micrometer-size overall structures of the interlaced nanoflake-assembled flower-like hierarchical Ag/Cu_2O composite microspheres enable them to be recycled and reused easily from solution by natural settlement in a short time.

2 Experimental sections

2.1 Synthesis of interlaced nanoflake-assembled flower-like hierarchical Ag/Cu_2O composite microspheres

All reagents are of analytical grade and used without further purification. $Cu(NO_3)_2 \cdot 3H_2O$ (99.0–102.0%), $AgNO_3$ (≥99.8%), polyvinylpyrrolidone (PVP, $M_w \approx$ 45 000–58 000, water content ≤ 5.0%), ethylene glycol (EG, water content ≤ 0.1%), absolute ethanol (water content ≤ 0.3%) and hydrogen peroxide (H_2O_2, ≥30.0%) were purchased from Sinopharm Chemical Reagent Co., Ltd., China. Methyl Orange (MO) was purchased from Tianjin Kemiou Chemical Reagent Co., Ltd., China. Deionized water was made in our lab.

The sample was synthesized *via* a one-step solvothermal method, and the details are as follows: $Cu(NO_3)_2 \cdot 3H_2O$ (1.5 mmol), $AgNO_3$ (0.252 mmol) and polyvinylpyrrolidone (PVP, 0.2 g) were added into ethylene glycol (30 mL) under constant magnetic stirring (500 rpm) at room temperature for 1 h. The color of the solution was turned to pure blue. Then, the pure blue solution was transferred into a Teflon-skinned autoclave (50 mL capacity) and heated at 180 °C for 1 h. After the reaction system was naturally cooled to room temperature, the brownish black precipitates was separated from solution and thoroughly washed for several times with deionized water and absolute ethanol to remove the impurities, and then dried in a vacuum oven (pressure (relative vacuum degree) = −0.085 MPa) at 60 °C for 12 h.

2.2 Photocatalytic properties

The catalytic activity experiments of the obtained products for the oxidation and decoloration of the Methyl Orange (MO) dye under visible light illumination were carried out at ambient temperature. In our experiment, 40 mg of the obtained products were dispersed in 40 mL of MO aqueous solution (30 mg L^{-1}). The catalyst/substrate ratio is 33.3 mg catalyst per mg substrate in our model reactions. Before illumination, the mixed solution was magnetically stirred in the dark for 20 min to ensure the establishment of an adsorption–desorption equilibrium and then followed by standing for 10 min. Then, the dispersion was irradiated by a 500 W xenon lamp under magnetic stirring (500 rpm, the distance between the dispersion and xenon lamp is 10 cm). At given time intervals, the dispersion was sampled and centrifuged to separate the catalyst. The concentration of MO in the solution was determined at different intervals using a UV/vis/NIR spectrophotometer (Hitachi U-4100). In addition, we have also studied the effect of the hydrogen peroxide solution (H_2O_2, 30% wt) on the photocatalytic degradation of MO aqueous solution.

2.3 Characterization

Powder X-ray diffraction (XRD) patterns were obtained in the 2θ range of 15–85° using a Philips X'Pert Pro X-ray diffractometer with Cu Kα radiation (1.5418 Å). The scanning electron microscope (SEM) images were taken on a SEM (JEOL-6610-LV), equipped with X-ray energy dispersive spectroscopy (EDS, X-Max, Oxford Instruments) capabilities, working at an

accelerating voltage of 10.0 kV. The transmission electron microscope (TEM) and high resolution transmission electron microscope (HRTEM) analysis images were performed on a JEOL JEM-2100 transmission electron microscope operating at an accelerating voltage of 200 kV. The X-ray photoelectron spectroscopy (XPS) was collected on the ESCALab MKII X-ray photoelectron spectrometer (K-Alpha 1063). Photoluminescence (PL) spectra were tested on a F280 fluorescence spectrophotometer. The UV-vis spectra were measured by a UV/vis/NIR spectrophotometer (Hitachi U-4100).

3 Results and discussion

3.1 Structure and morphology of interlaced nanoflake-assembled flower-like hierarchical Ag/Cu_2O composite microspheres

The composition and phase purity of the as-prepared product are carried out by X-ray diffraction (XRD). The obtained pattern is identified through comparison with standard Cu_2O and Ag patterns. As shown in Fig. 1(a), the diffraction peaks center at 2θ values of 29.64, 36.52, 42.42, 61.55, 69.78, 73.73 and 77.60° are agree with (110), (111), (200), (220), (310), (311) and (222) crystal planes of the cubic Cu_2O (JCPDS card no. 77-0199) phase, and the other diffraction peaks at $2\theta = 38.26$, 44.47, 64.71, 77.73 and 81.90 are corresponded to (111), (200), (220), (311) and (222) crystal planes of cubic Ag (JCPDS card no. 87-0718) phase. The XRD pattern of the as-prepared Ag/Cu_2O product shows the coexistence of Ag and Cu_2O, and no additional peaks are detected. The results clearly illustrate the high purity of the as-prepared Ag/Cu_2O product. Scanning electron microscopy (SEM) image of the as-prepared Ag/Cu_2O product (Fig. 1(b) and (c)) shows that it consists of many monodispersed and uniform Ag/Cu_2O composite microspheres with a diameter of approximately 4–5 μm. The detailed morphology of the microspheres is shown in Fig. 1(d), which reveals that it has interlaced nanoflake-assembled flower-like hierarchical structure. In addition, the flower-like hierarchical structure is composed of interlaced nanoflakes with a thickness of 80–90 nm. The as-prepared microspheres are monodispersed and can be well dispersed in the solution without large aggregation (Fig. 1(a) and (b)).

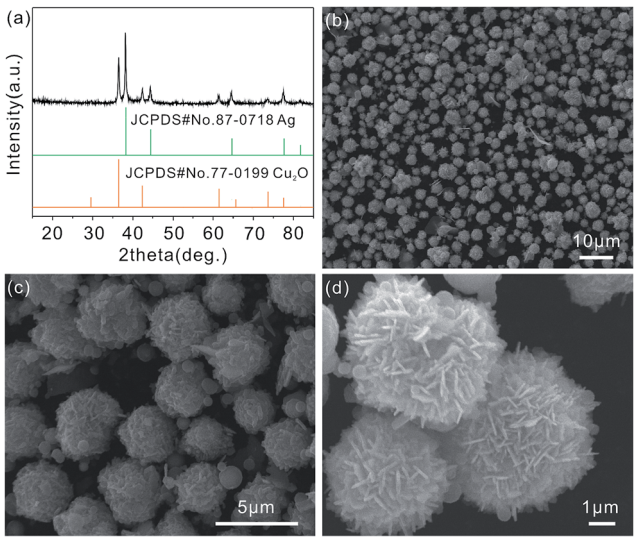

Fig. 1 XRD pattern (a) and SEM images (b–d) of the flower-like hierarchical Ag/Cu_2O composite microspheres.

In order to obtain detailed information about Ag and Cu_2O distributions in the flower-like hierarchical Ag/Cu_2O composite microspheres, the product is also analyzed by electron mapping image analysis (Fig. 2(a–d)). The images are acquired by visualizing the inelastically scattered electrons in the energy loss windows for elemental Cu, Ag, and O. The different color areas shown in parts (b–d) of Fig. 2 indicate Cu-, Ag-, and O-enriched areas of the product, respectively. The images show that the elemental Cu and Ag are well dispersed on the surface of the flower-like hierarchical Ag/Cu_2O composite microspheres. Fig. 2(e) shows EDS spectrum of the product, in which the Cu, Ag, and O elements is observed. Transmission electron microscopy (TEM) is also used to characterize the flower-like hierarchical Ag/Cu_2O composite microspheres. The nanoflakes, constructing the hierarchical composite microsphere, are transparent to electron beam (Fig. 2(f)). In some areas, the nanoflake is oriented approximately perpendicular to the plane of the supporting copper TEM grid (marked by black arrow in Fig. 2(f)), from which the thickness of the nanoflake is estimated to be around 110 nm. A typical high resolution transmission electron microscopy (HRTEM) image of Ag/Cu_2O heterostructures (as shown in Fig. 2(g)) reveal that the metallic Ag nanoparticles with a diameter of 5–10 nm (indicated by orange dotted circles in Fig. 2(g)) attach on the surface of Cu_2O nanoflakes. The HRTEM image also shows the interplanar spacing of 0.24 nm and 0.23 nm (marked by white lines and arrows), which correspond to (111) lattice planes of Cu_2O and (111) lattice planes of Ag, respectively.

The surface components and chemical states of the flower-like hierarchical Ag/Cu_2O composite microspheres are investigated by XPS analysis and the corresponding results are shown in Fig. 3. The survey spectrum shows the silver peaks (Ag 3d), the copper photoelectron peaks (Cu 3s, Cu 2p, Cu 3p, and its Cu LMM Auger), the oxygen peaks (O 1s) and the photoelectron peak of the adventitious carbon (C 1s). The appearance of C peak mainly comes from pump oil due to vacuum treatment before the XPS test. No other peaks can be observed, indicating that the composite microspheres are composed of Cu, Ag and O.

High-resolution spectra of Ag, Cu and O species are shown in Fig. 3(b–d), respectively. Fig. 3(b) shows the Ag 3d XPS spectrum for the composite microspheres. Two peaks located at 374.0 eV and 368.1 eV are attributed to Ag $3d_{3/2}$ and Ag $3d_{5/2}$, respectively. Peak positions of Ag 3d are close to that of pure metallic Ag.[34] In addition, the binding energy of Ag 3d shifts to a lower binding energy compared with the corresponding value of the bulk Ag (368.2 and 374.2 eV, respectively), due to the interaction between the Ag and Cu_2O microcrystals. The XPS spectrum shown in Fig. 3(c) demonstrates the Cu $2p_{1/2}$ and Cu $2p_{3/2}$ spin–orbital photoelectrons located at binding energies of 950.1 eV and 930.3 eV, respectively, which are in good agreement with the reported values of Cu_2O.[35,36] From Fig. 3(d), the O 1s profile

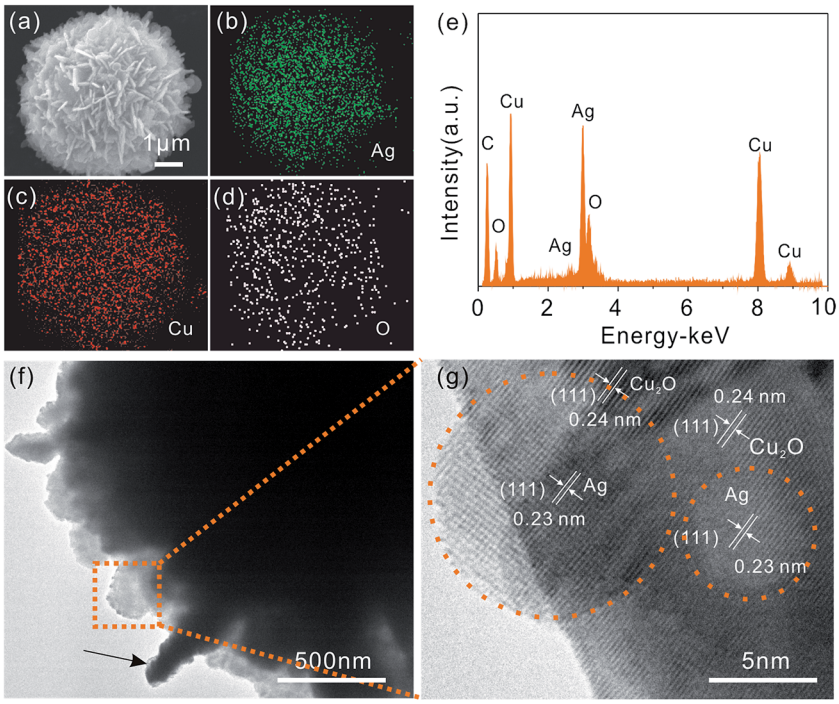

Fig. 2 SEM image (a) and EDS spectrum (e) of the flower-like hierarchical Ag/Cu_2O composite microspheres. Element mapping images of the flower-like hierarchical Ag/Cu_2O composite microspheres with "Ag" (b), "Cu" (c), and "O" (d). TEM (f) and HRTEM (g) images of the flower-like hierarchical Ag/Cu_2O composite microspheres. The black arrow in (f) marks that the nanoflake is oriented approximately perpendicular to the plane of the supporting copper TEM grid.

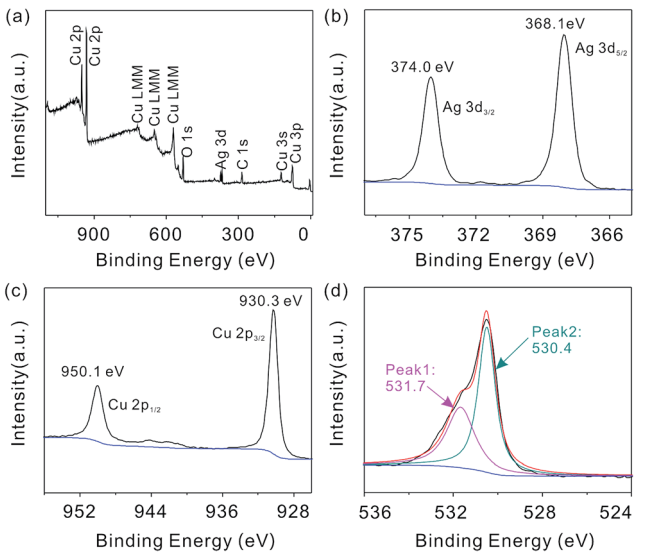

Fig. 3 XPS spectrum of the flower-like hierarchical Ag/Cu_2O composite microspheres (a); and the high-resolution spectra of Ag 3d (b), Cu 2p (c) and O 1s (d).

is asymmetric and can be fitted into two symmetrical peaks located at 531.7 (Peak 1) and 530.1 eV (Peak 2). The fitted peaks are originated from the lattice oxygen of adsorbed oxygen and Cu_2O, respectively.[37,38] The XRD, EDS and XPS (as shown in Fig. 1(a), 2(e) and 3) results consistently prove the formation of Ag and Cu_2O.

3.2 Effect of the molar ratio of $Cu(NO_3)_2 \cdot 3H_2O$ to $AgNO_3$ on the phase composition of the final products

The effect of the molar ratio of $Cu(NO_3)_2 \cdot 3H_2O$ to $AgNO_3$ on the phase composition of the final products has been conducted in our experiments. During these experiments, the molar ratios of $Cu(NO_3)_2 \cdot 3H_2O$ to $AgNO_3$ are tuned from 2.0 mmol/0.376 mmol (named Sample 1), 2.0 mmol/0.500 mmol (named Sample 2), to 1.5 mmol/0.252 mmol (named Sample 3), while the volume of EG, the amount of PVP, reaction temperature and reaction time is fixed at 30 mL, 0.2 g, 180 °C and 1 h, respectively. As shown in Fig. 4(a), the flower-like hierarchical microspheres with a diameter about 3–4 μm are obtained when the molar ratio of $Cu(NO_3)_2 \cdot 3H_2O$ to $AgNO_3$ is 2.0 mmol/0.376 mmol. Under the molar ratio of 2.0 mmol/0.5 mmol, the flower-like hierarchical microspheres are still able to be prepared (Fig. 4(b)). When the molar ratio is 1.5 mmol/0.252 mmol, the flower-like hierarchical microspheres are also prepared successfully (Fig. 1). Thus, the molar ratio of $Cu(NO_3)_2 \cdot 3H_2O$ to $AgNO_3$ is not obviously effect on the morphology. The corresponding XRD patterns of the Sample 1 and 2 are shown in Fig. 4(c) and (d), respectively. From the figures, it is clear that the coexistence of Ag and Cu_2O. In addition, impure diffraction peaks are also detected (marked by purple inverted triangles). After careful analysis, these impure diffraction peaks can be indexed to the pattern of copper (Cu) according to JCPDS card no. 70-3038, as shown in Fig. 4(c) and (d). In addition, the exact contents of Cu in Sample 1 and 2 are 1 wt% and 3 wt%, respectively. In our experiments, we have also systematically studied the effect of the reaction time on the

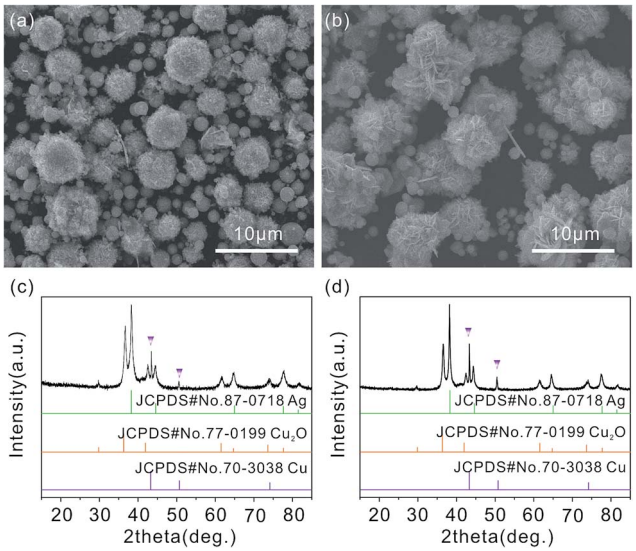

Fig. 4 SEM images of products obtained under different $Cu(NO_3)_2 \cdot 3H_2O/AgNO_3$ molar ratios: (a) Sample 1 with 2.0 mmol $Cu(NO_3)_2 \cdot 3H_2O$ and 0.376 mmol $AgNO_3$; (b) Sample 2 with 2.0 mmol $Cu(NO_3)_2 \cdot 3H_2O$ and 0.5 mmol $AgNO_3$; (c) and (d) the corresponding XRD patterns of the above samples. Other parameters are fixed, including 30 mL EG, 0.2 g PVP, $T = 180$ °C and $t = 1$ h.

formation of the flower-like hierarchical Ag/Cu_2O composite microspheres. The results indicate that the morphologies and phase purities of the obtained products can be regulated by the reaction time. And the detailed contents are shown in ESI (Fig. S1†).

3.3 Optical properties of Ag/Cu_2O composites

The UV-vis diffuses reflectance spectra of the flower-like hierarchical Ag/Cu_2O composite microspheres, the Ag/Cu_2O-1 wt% Cu and the Ag/Cu_2O-3 wt% Cu are shown in Fig. 5(a). According to the Kubelka–Munk equation: $\alpha = (1 - R)^2/2R$, where R is the reflection coefficient of the product, $R = 10^{-A}$, A is an optical absorption. The optical band gap (E_g) can be related to absorption coefficient (α) by the following equation:[39]

$$\alpha h\nu = \text{const}(h\nu - E_g)^2$$

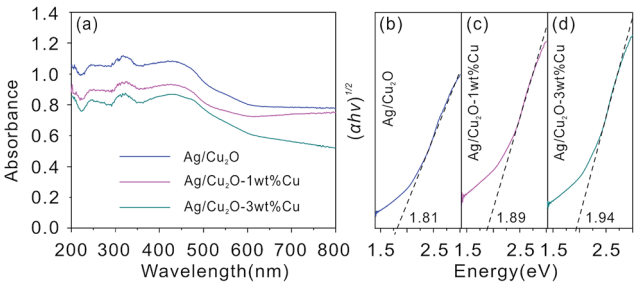

Fig. 5 (a) The UV-vis diffuses reflectance spectra for the flower-like hierarchical Ag/Cu_2O composite microspheres (Sample 3), Ag/Cu_2O-1 wt% Cu (Sample 1) and Ag/Cu_2O-3 wt% Cu (Sample 2). (b)–(d) The corresponding $(\alpha h\nu)^2$ *versus* energy ($h\nu$) plots of the above samples.

Fig. 5(b)–(d) plots the relationship of $(\alpha h\nu)^{1/2}$ *versus* energy ($h\nu$) of the products and the optical band gap is the extrapolated value. Obviously, the band gap of Ag/Cu_2O composites is 1.81 eV, whereas the band gaps of the Ag/Cu_2O-1 wt% Cu and Ag/Cu_2O-3 wt% Cu composites has been slightly increased to 1.89 and 1.94 eV, respectively. The flower-like hierarchical Ag/Cu_2O composite microspheres show a broad and strong absorbance in the visible light region due to its narrow band gap (1.81 eV). However, when there are some Cu contents in the Ag/Cu_2O composites, the Ag/Cu_2O-1 wt% Cu and Ag/Cu_2O-3 wt% Cu exhibit not only a blue shift in the absorption edge but also a weak absorption in the visible light range. This indicates that the appearance of Cu in the products obviously inhibit the light absorption properties of Ag/Cu_2O composites. Furthermore, the absorption intensity is also found to gradually decrease with increasing Cu content. Therefore, good photocatalytic activity of the flower-like hierarchical Ag/Cu_2O composite microspheres under visible light illumination is expected.

3.4 Photocatalytic properties of Ag/Cu_2O composites

In the current work, the photocatalytic decomposition of MO is used to evaluate the photocatalytic activity of the flower-like hierarchical Ag/Cu_2O composite microspheres under visible light illumination at room temperature. A control experiment without any catalyst (blank experiment), commercial Cu_2O, the Ag/Cu_2O-1 wt% Cu and Ag/Cu_2O-3 wt% Cu composites are used for comparison. Absorbance, an indication of MO concentration, is used to measure the extent of MO dye decomposition. The characteristic absorption peak at 464 nm of MO is monitored to follow the catalytic degradation process. The ratio C/C_0 is used to describe the degradation, which stands for the concentration ratio after and before a certain reaction time.

Fig. 6(a) summarizes the activities of the photocatalyst toward MO degradation through monitoring the adsorption intensity at 464 nm *versus* time. Before visible light illumination, the mixed solution containing the catalyst and MO is stirred in the dark for 20 min to ensure that MO is adsorbed to saturation on the surface of catalysts. In the control experiment without any catalyst (blank experiment, curve (i) in Fig. 6(a)), C/C_0 (relative concentration) of MO is degraded by only 0.04% after visible light illumination for 20 min (Fig. 6(c), Panel i). A photocatalytic test is also conducted using commercial Cu_2O under the same conditions as aforementioned (curve (ii) in Fig. 6(a)). It can be seen that about 3.36% of the MO is degraded after 20 min (Fig. 6(c), Panel ii). Further experiment is carried out to compare the photocatalytic properties of the flower-like hierarchical Ag/Cu_2O composite microspheres, the Ag/Cu_2O-1 wt% Cu and Ag/Cu_2O-3 wt% Cu. Under the same conditions, the flower-like hierarchical Ag/Cu_2O composite microspheres illustrate a higher photocatalytic activity (curve (iii) in Fig. 6(a)) than the Ag/Cu_2O-1 wt% Cu (curve (iv) in Fig. 6(a)) and the Ag/Cu_2O-3 wt% Cu (curve (v) in Fig. 6(a)). About 81.2% of the MO is degraded by the flower-like hierarchical Ag/Cu_2O composite microspheres (Fig. 6(c), Panel iii) after 20 min; by contrast, the Ag/Cu_2O-1 wt% Cu decompose the MO to 66.3% after 20 min (Fig. 6(c), Panel iv) and the Ag/Cu_2O-3 wt% Cu decompose the

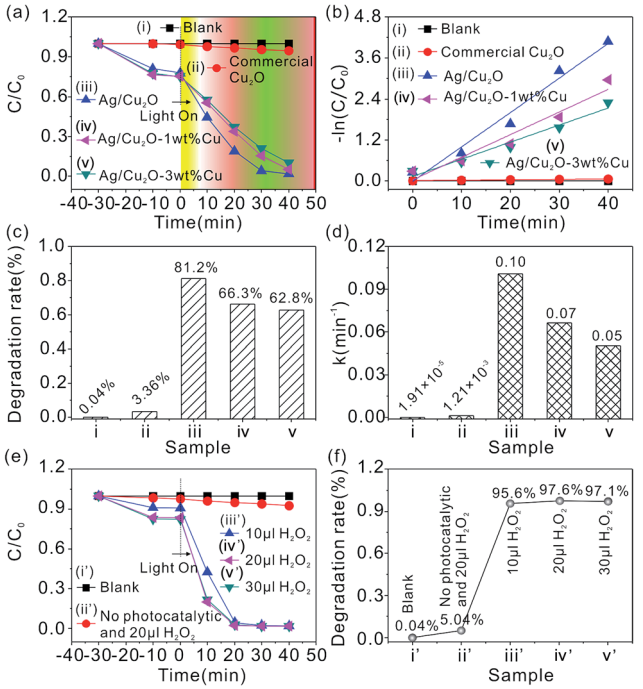

Fig. 6 (a) The kinetic curve of photodegradation of MO solution by different catalysts under visible light illumination. (b) Comparison of first-order degradation rates for MO degradation by different catalysts. (c) A plot of the extent of photodegradation of MO by different catalysts after visible light illumination for 20 min, Panel i: without any catalyst (blank experiment), Panel ii: commercial Cu_2O, Panel iii: flower-like hierarchical Ag/Cu_2O composite microspheres, Panel iv: Ag/Cu_2O-1 wt% Cu, Panel v: Ag/Cu_2O-3 wt% Cu. (d) Calculated pseudo first order constants, k (min^{-1}), for different catalysts. (e) The kinetic curve of photodegradation of MO solution by the flower-like hierarchical Ag/Cu_2O composite microspheres under visible light in the presence of different amounts of H_2O_2. (f) Effect of H_2O_2 concentrations on degradation rate of MO after visible light illumination for 20 min.

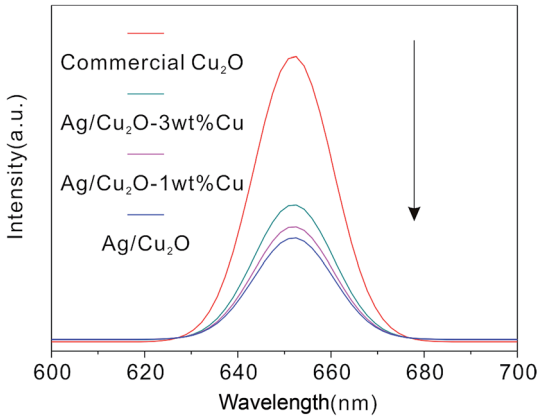

Fig. 7 PL spectra of commercial Cu_2O, Ag/Cu_2O, Ag/Cu_2O-1 wt% Cu and Ag/Cu_2O-3 wt% Cu with an excitation wavelength of 325 nm.

MO to 62.8% after 20 min (Fig. 6(c), Panel v). From experimental results, this indicates that the existence of Cu in the products does not favor high photocatalytic activity for Ag/Cu_2O composites. The photocatalytic activity gradually decreases with increasing Cu content.

The photoluminescence (PL) technique is an effective way to study the efficiency of charge carrier trapping, immigration and transfer. A lower PL intensity usually implies a lower electron–hole recombination rate and higher photocatalytic activity.[40] Fig. 7 shows the measured PL emission spectra of the as-prepared structures at an excitation wavelength of 325 nm, which is higher than the band gap of Cu_2O. It is clearly observed that the commercial Cu_2O display a strong PL intensity at around 650 cm^{-1}, which should be the near band emission of Cu_2O.[41] After the Ag is combined with the Cu_2O, the PL intensity shows an apparent decrease, indicating that the recombination of the excitons in Cu_2O is efficiently hampered. However, in the case of Ag/Cu_2O-1 wt% Cu, evidently the PL intensity is increased compared to Ag/Cu_2O, suggesting that Cu inhibits the photogenerated electrons trapped by Ag, thereby resulting in the PL intensity increasing. Moreover, it is noted that the PL intensity of Ag/Cu_2O-1 wt% Cu is also lower than Ag/Cu_2O-3 wt% Cu. Based on the above results, it is concluded that the existence of excess Cu in the products provides the recombination centers for electron–hole pairs[42,43] and thereby the Ag/Cu_2O shows more effective charge separation. As displayed in Fig. 7, the PL intensity follows the order: Ag/Cu_2O < Ag/Cu_2O-1 wt% Cu < Ag/Cu_2O-3 wt% Cu < commercial Cu_2O, which is greatly consistent with the photocatalytic results.

The photodegradation of MO can be described as pseudo first order: $\ln(C/C_0) = -kt$, where C_0 and C are MO concentrations initially and after time t, respectively, and the rate constants (k, min^{-1}) are determined from plots of $\ln(C/C_0)$ *versus* illumination time. Fig. 6(b) shows the linear relationship represented by the $\ln(C/C_0)$ *versus* reaction time t for different catalysts employed in our work. The apparent reaction rate constant (k) can be calculated from the rate equation $\ln(C/C_0) = -kt$. The reaction rate constants for the photodegradation of MO are $k_i = 1.91 \times 10^{-5}$, $k_{ii} = 1.21 \times 10^{-3}$, $k_{iii} = 0.1$, $k_{iv} = 0.07$ and $k_v = 0.05$ min^{-1} for the blank experiment, the commercial Cu_2O, the flower-like hierarchical Ag/Cu_2O composite microspheres, the Ag/Cu_2O-1 wt% Cu and Ag/Cu_2O-3 wt% Cu composites, respectively (Fig. 6(d)). From the results, the kinetic reaction constants k of MO photodegradation in the presence of the flower-like hierarchical Ag/Cu_2O composite microspheres is 121, 1.43 and 2 times faster than that of the reaction in the presence of the commercial Cu_2O, the Ag/Cu_2O-1 wt% Cu and the Ag/Cu_2O-3 wt% Cu composites, respectively. Table 1 summarizes the photocatalytic degradation capacity of various photocatalysts for MO. It is found that the photocatalytic degradation capacity of the flower-like hierarchical Ag/Cu_2O composite microspheres is lower than that of nanoscale Cu_2O. Even though, the photocatalytic degradation capacity of the flower-like hierarchical Ag/Cu_2O composite microspheres for MO is still better than that of other previously reported Ag/Cu_2O composites and some other related semiconductor photocatalyst materials.

Fig. 6(e) shows the effect of H_2O_2 dosage on the photocatalytic activity of the flower-like hierarchical Ag/Cu_2O composite microspheres. As shown in Fig. 6(e), the photodegradation rates

Table 1 Comparison of our work with nanoscale Cu_2O, some Ag/Cu_2O composites and other semiconductor photocatalysts reported

Catalysts	Degradation time	Degradation percentage	Ref.
Interlaced nanoflake-assembled flower-like hierarchical Ag/Cu_2O composite microspheres	20 min	81.3%	This study
Ag/Cu_2O-1 wt% Cu	20 min	66.3%	
Ag/Cu_2O-3 wt% Cu	20 min	62.8%	
Commercial Cu_2O	20 min	3.36%	
Hierarchical Cu_2O nanospheres	10 min	98.1%	46
Porous Cu_2O nanospheres	20 min	95.8%	47
Ag@Cu_2O core–shell heteronanowires	20 min	75.1%	31
Ag–Cu_2O composites	20 min	77.8%	48
Reduced graphene oxide supported Ag–Cu_2O composites with hierarchical structures	20 min	71.5%	49
Ag–Cu_2O nanocorncobs	60 min	68.8%	50
Cu_2O/Ag composite nanospheres	60 min	78.9%	51
Copper(II)-based high-connected metal–organic frameworks	20 min	56.8%	52
Pd cocatalyst on Sm-doped $BiFeO_3$ nanoparticles	60 min	62.2%	53
Novel tungstosilicic acid immobilized on zeolites catalyst	120 min	58.8%	54
Pine tree-like Cu/ZnO heterostructured film	120 min	68.5%	55
WO_3/TiO_2 nanowires	160 min	50.2%	56

(C/C_0) of MO can be neglected after visible light illumination for 20 min in the blank experiment (curve (i′), and (Fig. 6(e), Sample i′)), and only 20 μL H_2O_2 (curve (ii′), and (Fig. 6(e), Sample ii′)). However, when the flower-like hierarchical Ag/Cu_2O composite microspheres are added in this reaction system in the presence of H_2O_2, the photodegradation rates of MO are over 95% after visible light illumination for 20 min (Fig. 6(e), curve (iii′), curve (iv′) and curve (v′)). Compared with the condition without adding H_2O_2 (Fig. 6(c), Panel iii), the photocatalytic degradation rates of MO increase to over 14.4% after 20 min illumination. The results suggest that the addition of small amounts of H_2O_2 can accelerate the photodegradation rate of the flower-like hierarchical Ag/Cu_2O composite microspheres.[44] It is possible that more radicals are formed in the presence of H_2O_2, thus leading to an increase of the photodegradation rate.[45]

The degradation rate *versus* different initial dosage of H_2O_2 has been shown in Fig. 6(f). From the figure, when the initial dosage of H_2O_2 is 10 μL, the flower-like hierarchical Ag/Cu_2O composite microspheres display the lowest photodegradation rate (about 95.6%). When the concentration of H_2O_2 is 20 μL (Sample iv′), the photodegradation rate reaches a maximum (about 97.6%). When the dosage of H_2O_2 is further increased to 30 μL (Sample v′), the photodegradation rate begins to decrease (about 97.1%). The results suggest that an optimum dosage of H_2O_2 can be 20 μL. At low dosages of H_2O_2, the number of hydroxyl radicals (˙OH radicals) increase when increasing the dosages of H_2O_2, so the degradation rate of MO enhances correspondingly. However, excess H_2O_2 can result in a self-consumption and scavenging effect of ˙OH radical through the reaction described by eqn (1) and (2); at the same time, ˙OH radicals can also dimerize to H_2O_2 by eqn (3) at high dosage.[57–61]

$$H_2O_2 + {}^{\cdot}OH \rightarrow {}^{\cdot}HO_2 + H_2O \quad (1)$$

$$^{\cdot}HO_2 + {}^{\cdot}OH \rightarrow O_2 + H_2O \quad (2)$$

$$^{\cdot}OH + {}^{\cdot}OH \rightarrow H_2O_2 \quad (3)$$

Catalyst stability and reusability are of vital importance in practical applications. The photocatalytic activity for the flower-like hierarchical Ag/Cu_2O composite microspheres in degradation of MO is studied in consecutive cycles (90 min illumination for each cycle) and shows in Fig. 8(a). From the results obtained,

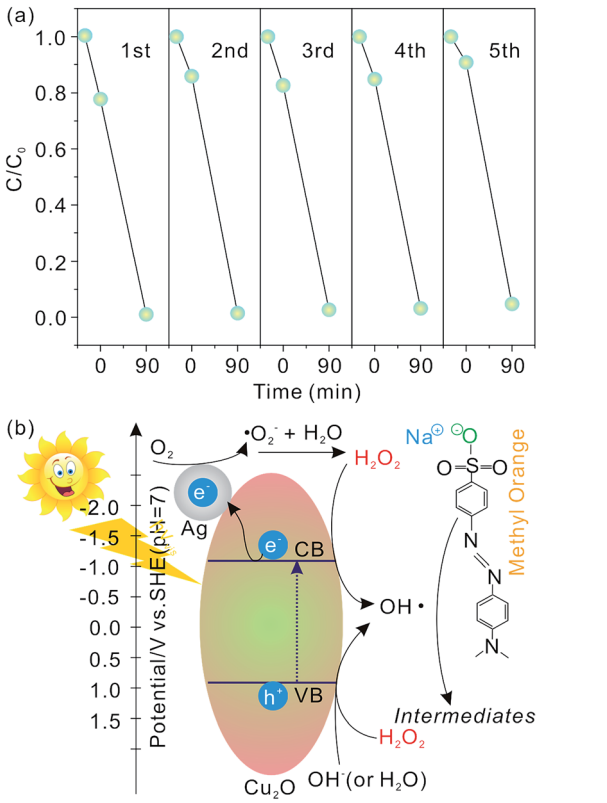

Fig. 8 (a) Photodegradation properties of the flower-like hierarchical Ag/Cu_2O composite microspheres toward MO solution within five cycles under visible light illumination; (b) schematic of photo-activation of the flower-like hierarchical Ag/Cu_2O composite microspheres and degradation of MO.

it is observed that over 98.97% of MO is photodegraded when the flower-like hierarchical Ag/Cu_2O composite microspheres are used for the first time. After five consecutive cycles, 95.26% of MO is photodegraded, the photocatalytic activity of the flower-like hierarchical Ag/Cu_2O composite microspheres almost remain unchanged, indicating that they are photostable during the photodegradation of MO. Furthermore, such micrometer-sized overall structures of the flower-like hierarchical Ag/Cu_2O composite microspheres enable them to be recycled and reused easily from solution by natural settlement in a short time.

A possible photocatalysis mechanism for the flower-like hierarchical Ag/Cu_2O composite microspheres is illustrated in Fig. 8(b). When the flower-like hierarchical Ag/Cu_2O composite microspheres are illuminated by visible light with photon energy higher than the band gap of Cu_2O, electrons in the valence band (VB) can be excited to the conduction band (CB), leaving behind the same amount of holes in VB. As the work function of Ag (4.6 eV) is greater than that of Cu_2O (4.2 eV),[62,63] electrons hence can be transferred from the CB of Cu_2O to Ag.[1,64] The holes in the VB can be trapped by the OH^- (or H_2O), resulting in the formation of $^{\bullet}OH$ radical species.[65] The electrons can be captured by the adsorbed O_2 and form the superoxide anion radicals ($^{\bullet}O_2^-$ radicals). The $^{\bullet}O_2^-$ radicals can ultimately be reduced to $^{\bullet}OH$ radicals.[66] It is known that the $^{\bullet}OH$ radicals are able to oxidize pollutants due to their high oxidative capacity. Hence, under visible light illumination, MO molecules can be photodegraded by the flower-like hierarchical Ag/Cu_2O composite microspheres. When H_2O_2 is added in the reaction system, the electrons and holes can be also captured by H_2O_2 molecules, leading to the formation of more $^{\bullet}OH$ radicals, as shown in Fig. 8(b), which is in favor of oxidizing MO molecules. Thus, an appropriate dosage of H_2O_2 can accelerate the photocatalytic activity of the flower-like hierarchical Ag/Cu_2O composite microspheres.

4 Conclusion

In summary, we have synthesized the interlaced nanoflake-assembled flower-like hierarchical Ag/Cu_2O composite microspheres *via* a one-step, environmentally friendly solvothermal method. Influencing factors, such as the molar ratio of $Cu(NO_3)_2 \cdot 3H_2O$ to $AgNO_3$, play important roles in the contents of Cu in the obtained products. The as-prepared interlaced nanoflake-assembled flower-like hierarchical Ag/Cu_2O composite microspheres exhibit better photocatalytic properties in photodegradation of MO compared with the commercial Cu_2O. Our experimental results for photodegradation of MO also indicate that the existence of Cu in the products does not favor high photocatalytic activity for Ag/Cu_2O composites. The photocatalytic activity gradually decreases with increasing Cu content. It may be due to the existence of excess metal in the products which provides the recombination centers for electron–hole pairs. The addition of small amounts of H_2O_2 can further accelerate the photodegradation rate of the interlaced nanoflake-assembled flower-like hierarchical Ag/Cu_2O composite microspheres. After five consecutive cycles, the photocatalytic activity of the interlaced nanoflake-assembled flower-like hierarchical Ag/Cu_2O composite microspheres almost remain unchanged, indicating that they are photostable during the photodegradation of MO. Most importantly, such micrometer-sized overall structures of the interlaced nanoflake-assembled flower-like hierarchical Ag/Cu_2O composite microspheres enable them to be recycled and reused easily from solution by natural settlement in a short time. These results suggest that the interlaced nanoflake-assembled flower-like hierarchical Ag/Cu_2O composite microspheres had potential applications in visible light photocatalysis for environmental remediation.

Acknowledgements

This research was supported by the National Natural Science Foundation of China (51302102, 51402120, 51571166 and 61505167), the Key Natural Science Research Project for Colleges and Universities of Anhui Province (KJ2016A638, KJ2016SD53 and KJ2014B11), the Natural Science Foundation of Anhui Province (1708085ME96), the Huaibei Scientific Talent Development Scheme (20140305 and 20140318), the Huaibei Normal University youth research project (2014xq017). We also thank the support of the Natural Science Research Project of Shaanxi Province (2016JM5001), the Research Fund of the State Key Laboratory of Solidification Processing (NWPU) (Grant No. 147-QZ-2016), The Research Fund of Key Laboratory of Materials Physics, Institute of Solid State Physics, CAS (2016KLMP04), and the Key Scientific and Technological Team from Shaanxi Province (No. 2015KCT-12).

References

1 H. Wang, L. Zhang, Z. Chen, J. Hu, S. Li, Z. Wang, J. Liu and X. Wang, *Chem. Soc. Rev.*, 2014, **43**, 5234–5244.
2 K. Maeda, *ACS Catal.*, 2013, **3**, 1486–1503.
3 D. J. Martin, G. G. Liu, S. J. A. Moniz, Y. P. Bi, A. M. Beale, J. H. Ye and J. W. Tang, *Chem. Soc. Rev.*, 2015, **44**, 7808–7828.
4 X. Li, S. Guo, C. Kan, J. Zhu, T. Tong, W. Choy and B. Wei, *Nano Energy*, 2016, **30**, 549–558.
5 Y. Zhang, Y. Ye, X. Zhou, Z. Liu, D. Ma, B. Li, Q. Liu, G. Zhu, S. Chen and X. Li, *CrystEngComm*, 2016, **18**, 7994–8003.
6 X. Li, J. Zhu and B. Wei, *Chem. Soc. Rev.*, 2016, **11**, 3145–3187.
7 Y. Zhong, Z. Wang, R. Zhang, F. Bai, H. Wu, R. Haddad and H. Fan, *ACS Nano*, 2014, **8**, 827–833.
8 R. Xie, G. Fan, L. Yang and F. Li, *Catal. Sci. Technol.*, 2015, **5**, 540–548.
9 M.-H. Sun, S.-Z. Huang, L.-H. Chen, Y. Li, X.-Y. Yang, Z.-Y. Yuan and B.-L. Su, *Chem. Soc. Rev.*, 2016, **45**, 3479–3563.
10 X. Li, J. Yu and M. Jaroniec, *Chem. Soc. Rev.*, 2016, **45**, 2603–2636.
11 J.-S. Xu and Y.-J. Zhu, *CrystEngComm*, 2012, **14**, 2702–2710.
12 X. Zheng, Z. Han, S. Yao, H. Xiao, F. Chai, F. Qu and X. Wu, *Dalton Trans.*, 2016, **45**, 7094–7103.
13 M. Li, K. Chang, T. Wang, L. Q. Liu, H. B. Zhang, P. Li and J. H. Ye, *J. Mater. Chem. A*, 2015, **3**, 13731–13737.

14 S. Guo, X. Li, J. Zhu, T. Tong and B. Wei, *Small*, 2016, **12**, 5692–5701.
15 C. Lu, L. Qi, J. Yang, X. Wang, D. Zhang, J. Xie and J. Ma, *Adv. Mater.*, 2005, **17**, 2562–2567.
16 H. Gao, J. Zhang, R. Wang and M. Wang, *Appl. Catal., B*, 2015, **172**, 1–6.
17 H.-Y. Jing, T. Wen, C.-M. Fan, G.-Q. Gao, S.-L. Zhong and A.-W. Xu, *J. Mater. Chem.*, 2014, **2**, 14563–14570.
18 J. Y. Xiang, J. P. Tu, Y. F. Yuan, X. H. Huang, Y. Zhou and L. Zhang, *Electrochem. Commun.*, 2009, **11**, 262–265.
19 N. Meir, I. Jenlaplante, K. Flomin, E. Chockler, B. Moshofsky, M. Diab, M. Volokh and T. Mokari, *J. Mater. Chem.*, 2013, **1**, 1763–1769.
20 C. Han, L. I. Zhiyu and J. Shen, *Asian J. Chem.*, 2015, **27**, 1861–1864.
21 B. Lu, A. Liu, H. Wu, Q. Shen, T. Zhao and J. Wang, *Langmuir*, 2016, **32**, 3085–3094.
22 L. Ye, Z. Li, X. Zhang, F. Lei and S. Lin, *J. Mater. Chem.*, 2014, **2**, 21010–21019.
23 M. R. Hoffmann, W. Choi and D. W. Bahnemann, *Chem. Rev.*, 1995, **95**, 69–96.
24 X. Z. Li and F. B. Li, *Environ. Sci. Technol.*, 2001, **35**, 2381–2387.
25 B. Chen, *J. Mater. Chem.*, 2012, **22**, 11651–11657.
26 F. Wenguang, J. Simon, S. Yiyi and M. K. H. Leung, *Phys. Chem. Chem. Phys.*, 2013, **16**, 676–680.
27 M. Zhao, H. Xu, S. X. Ouyang, D. W. Li, X. G. Meng and J. H. Ye, *Phys. Chem. Chem. Phys.*, 2016, **18**, 3409–3412.
28 Y. Bi and J. Ye, *Chem. Commun.*, 2009, 6551–6553.
29 Y. C. Chen, F. C. Zheng, Y. L. Min, T. Wang, Y. G. Zhang and Y. X. Wang, *J. Mater. Sci.: Mater. Electron.*, 2012, **23**, 1592–1598.
30 L. Li, X. Chen, Y. Wu, D. Wang, Q. Peng, G. Zhou and Y. Li, *Angew. Chem., Int. Ed.*, 2013, **52**, 11049–11053.
31 J. Xiong, Z. Li, J. Chen, S. Zhang, L. Wang and S. Dou, *ACS Appl. Mater. Interfaces*, 2014, **6**, 15716–15725.
32 J. Li, S. K. Cushing, J. Bright, F. Meng, T. R. Senty, P. Zheng, A. D. Bristow and N. Wu, *ACS Catal.*, 2013, **3**, 47–51.
33 Z. Wang, S. Zhao, S. Zhu, Y. Sun and M. Fang, *CrystEngComm*, 2011, **13**, 2262–2267.
34 W. Wei-Tai, W. Yusong, S. Lei, P. Wenmin, Z. Qingren, X. Guoyong and L. Fei, *J. Phys. Chem. B*, 2006, **110**, 14702–14708.
35 H. Qing, S. Daili, Z. Wenhua, C. Kai, C. Sujie, M. Yunsheng, J. Zhiquan, Y. Jinlong and H. Weixin, *Langmuir*, 2011, **27**, 665–671.
36 Z. Ai, L. Zhang, S. Lee and W. Ho, *J. Phys. Chem. C*, 2009, **113**, 20896–20902.
37 X. Lin, R. Zhou, J. Zhang and S. Fei, *Appl. Surf. Sci.*, 2009, **256**, 889–893.
38 G. Bacis, M. Catelani, L. Ciani, V. Scarano and R. Singuaroli, *Nanotechnology*, 2007, **18**, 1–4.
39 J. Cao, B. Xu, H. Lin, B. Luo and S. Chen, *Dalton Trans.*, 2012, **41**, 11482–11490.
40 J. Liqiang, Q. Yichun, W. Baiqi, L. Shudan, J. Baojiang, Y. Libin, F. Wei, F. Honggang and S. Jiazhong, *Sol. Energy Mater. Sol. Cells*, 2006, **90**, 1773–1787.
41 Y. Wang, S. Li, H. Shi and K. Yu, *Nanoscale*, 2012, **4**, 7817–7824.
42 B. Zhou, Z. Liu, H. Wang, Y. Yang and W. Su, *Catal. Lett.*, 2009, **132**, 75–80.
43 L. Ren, Y. P. Zeng and D. Jiang, *Catal. Commun.*, 2009, **10**, 645–649.
44 S. Sun, X. Zhang, J. Zhang, L. Wang, X. Song and Z. Yang, *CrystEngComm*, 2012, **15**, 867–877.
45 F. Ji, C. Li, J. Zhang and L. Deng, *Desalination*, 2011, **269**, 284–290.
46 S. Sun, X. Zhang, X. Song, S. Liang, L. Wang and Z. Yang, *CrystEngComm*, 2012, **14**, 3545–3553.
47 L. Zhang, B. Yu, P. Ying, L. Wu, S. Chen, J. Wang, X. Gu, R. Zhou and Z. Ni, *Superlattices Microstruct.*, 2015, **84**, 181–191.
48 J. Yang, Z. Li, C. Zhao, Y. Wang and X. Liu, *Mater. Res. Bull.*, 2014, **60**, 530–536.
49 L. Xu, F. Zhang, X. Song, Z. Yin and Y. Bu, *J. Mater. Chem. A*, 2015, **3**, 5923–5933.
50 S. Yang, S. Zhang, H. Wang, H. Yu, Y. Fang and F. Peng, *Mater. Res. Bull.*, 2015, **70**, 296–302.
51 W. Zhang, X. Yang, Z. Qian, K. Wang, J. Lu, C. Min and Z. Yang, *Ind. Eng. Chem. Res.*, 2014, **53**, 16316–16323.
52 G.-H. Cui, C.-H. He, C.-H. Jiao, J.-C. Geng and V. A. Blatov, *CrystEngComm*, 2012, **14**, 4210–4216.
53 S. Wang, D. Chen, F. Niu, N. Zhang, L. Qin and Y. Huang, *RSC Adv.*, 2016, **6**, 34574–34587.
54 C. L. Marchena, L. Lerici, S. Renzini, L. Pierella and L. Pizzio, *Appl. Catal., B*, 2016, **188**, 23–30.
55 K. Wang, Z. Chen, M. Huang, Z. Yang, C. Zeng, L. Wang, M. Qiu, Y. Zhang and W. Zhang, *RSC Adv.*, 2016, **6**, 103594–103600.
56 D. Nagy, T. Firkala, E. Drotár, A. Szegedi, K. Laszlo and I. M. Szilágyi, *RSC Adv.*, 2016, **6**, 95369–95377.
57 G. Granados-Oliveros, E. A. Páez-Mozo, F. M. Ortega, C. Ferronato and J. M. Chovelon, *Appl. Catal., B*, 2009, **89**, 448–454.
58 N. Daneshvar, M. A. Behnajady and Y. Z. Asghar, *J. Hazard. Mater.*, 2007, **139**, 275–279.
59 W. Luo, L. Zhu, N. Wang, H. Tang, M. Cao and Y. She, *Environ. Sci. Technol.*, 2010, **44**, 1786–1791.
60 E. Brillas, I. Sirés and M. A. Oturan, *Chem. Rev.*, 2009, **109**, 6570–6631.
61 D. D. Dionysiou, M. T. Suidan, E. Bekou, I. Baudin and J. M. Laîné, *Appl. Catal., B*, 2000, **26**, 153–171.
62 Y. Xu, *Am. Mineral.*, 2000, **85**, 543–556.
63 A. Henglein, *Berichte Der Bunsengesellschaft Für Physikalische Chemie*, 1997, **101**, 1562–1572.
64 Y. Pan, S. Deng, L. Polavarapu, N. Gao, P. Yuan, C. H. Sow and Q.-H. Xu, *Langmuir*, 2012, **28**, 12304–12310.
65 Y. Zheng, L. Zheng, Y. Zhan, X. Lin, A. Qi Zheng and K. Wei, *Inorg. Chem.*, 2007, **46**, 6980–6986.
66 W. Lu, S. Gao and J. Wang, *J. Phys. Chem. C*, 2008, **112**, 16792–16800.